Sustainable Food Technology

ROYAL SOCIETY OF CHEMISTRY

PAPER

View Article Online
View Journal

Cite this: DOI: 10.1039/d5fb00833f

Chitosan based ecofriendly nanoencapsulation formulation of *Clitoria ternatea* extract coated bacterial probiotic strain *Lactobacillus acidophilus*: a sustainable approach to improve probiotic functionality, stability, and tolerance

M. Lavanya and S. Karthick Raja Namasivayam *

In this study, a sustainable nanoencapsulation formulation of *Clitoria ternatea* extract-coated bacterial probiotic strain *Lactobacillus acidophilus* using nanoscale chitosan (CT-CS-LA-NC) was developed to enhance probiotic functionality, stability, and tolerance. The structural and functional characteristics of the nanocapsules were analyzed using scanning electron microscopy (SEM), Fourier transform infrared spectroscopy (FTIR), and thermogravimetric analysis (TGA). These analyses confirmed that the CT-CS-LA-NC nanocapsules were nanoscale in size, highly thermostable, and exhibited strong interactions among the polymer matrix, bacterial cell surface components, and plant extract. The encapsulation efficiency was found to be 98.43%, indicating effective preservation of viable probiotic cells during the encapsulation process. The antibacterial activity of CT-CS-LA-NC demonstrated significant inhibition against *Escherichia coli* and *Bacillus subtilis*. Antioxidant assessment revealed a free radical scavenging activity of 48.2 ± 1.32%. Under simulated gastric conditions (pH 2.5 and 3.5), the survivability of free and nanoencapsulated *L. acidophilus* showed notable differences after 36 hours. The encapsulated cells exhibited a higher survival rate of 60.93 ± 0.68% at pH 2.5, compared to only 21.29 ± 0.13% for free cells. Similarly, under bile tolerance conditions, encapsulated cells showed a survivability of 39.46 ± 0.68% at pH 2.5. Storage stability studies at 4 °C over 28 days revealed a rapid decline in the viability of free *L. acidophilus* cells, whereas CT-CS-LA-NC encapsulated cells maintained 94% viability after 7 days and 52% after 28 days. Molecular docking analysis using CB-Dock demonstrated strong binding affinities between anthocyanin, lactic acid, and chitosan ligands and gut-associated proteins such as O-GlcNAcase (7K41) and S-layer associated protein (SlpA) (8AE1), showing binding energies of −9.4 and −9.6 kcal mol^{-1}, respectively. Overall, the biocompatible and environmentally safe CT-CS-LA-NC formulation significantly improved probiotic stability during storage, enhanced survivability under harsh gastrointestinal conditions, and prolonged probiotic shelf life. These findings highlight its potential application as a sustainable ingredient for functional foods and nutraceutical formulations.

Received 31st October 2025
Accepted 17th February 2026

DOI: 10.1039/d5fb00833f

rsc.li/susfoodtech

Sustainability spotlight

This research introduces a sustainable and biocompatible nanoencapsulation strategy using chitosan and *Clitoria ternatea* extract to enhance the functionality, stability, and survivability of the probiotic strain *Lactobacillus acidophilus*. The developed CT-CS-LA-NC system integrates natural, renewable materials to improve probiotic tolerance under acidic and bile conditions, strengthen antibacterial and antioxidant properties, and extend storage stability without synthetic additives. By leveraging green biopolymers and plant-derived bioactives, this study contributes to the advancement of environmentally responsible probiotic delivery systems. The approach aligns with sustainable food innovation goals by promoting resource-efficient, safe, and functional probiotic formulations suitable for next-generation functional foods and nutraceuticals.

1. Introduction

Food spoilage is a significant issue affecting the economy and brand reputation of manufacturers. The food preservation and processing industry also seeks alternatives to conventional

Centre for Applied Research, Saveetha School of Engineering, Saveetha Institute of Medical and Technical Sciences (SIMATS), Chennai-602105, Tamil Nadu, India. E-mail: biologiask@gmail.com; Tel: +91 9842441198

preservatives.[1] The food industry is utilizing probiotic microorganisms, specifically lactic acid bacteria and bifidobacteria, as bio-preservatives to create healthy and safe food products.[2] These probiotics act as bio-preservatives, balancing beneficial and harmful bacteria in plant-based foods.[3,4] The FDA and WHO define probiotics as "live microorganisms which when administered in adequate amounts confer a health benefit on the host," which includes genera like *Saccharomyces*, *Bifidobacterium*, *Lactobacillus*, *Enterococcus*, *Bacillus*, *Escherichia*, and *Streptococcus*.[5,6]

Probiotics compete with harmful bacteria for adhesion sites, preventing colonization. They strengthen the intestinal barrier, reducing permeability and preventing harmful substances from entering the bloodstream.[7] Additionally, probiotics produce antimicrobial substances that inhibit pathogenic bacteria growth and can modulate the immune system to enhance defence mechanisms. Some probiotics also contribute to neurotransmitter synthesis, and influence the gut–brain communication.[8] Selecting the right probiotic strain is crucial for specific conditions. The amount consumed, formulation, and storage conditions are crucial for their effectiveness. Probiotics must survive the acidic stomach environment and small intestine bile. Quality control and shelf-life also impact the efficacy of probiotic products. Combining probiotics with prebiotics or other beneficial compounds can enhance their effects.[7,9] Among the crucial probiotic characteristics of *Lactobacillus acidophilus* that have been demonstrated *in vitro* and belong to the first group are antibiotic production, bile susceptibility, adaptability to low pH, adherence to human colon cells, lactase activity, and stability of the product. The latter group includes the general probiotic advantages observed in feeding studies at the animal level, such as immune response regulation, lowering serum cholesterol, improving lactose metabolism, and preventing or treating infections. When combined with chitosan-based antimicrobial preservatives, these probiotics can significantly enhance shelf life and food safety and maintain the quality of food products, presenting a natural and sustainable alternative to traditional preservation methods.[10] Among probiotic bacteria, *Lactobacillus acidophilus* is one of the more efficient types. Because of its advantageous properties, studies have indicated that it can be added to fermented foods. For *Lactobacillus acidophilus* to be effective as probiotics, it must adapt to the intestinal environment of the host and be viable and physiologically active at the target site in the host.[11]

Encapsulated probiotics are used in various products, and they are used to protect cores from degradation, reduce evaporation, improve material handling, and enhance the stability of the active ingredients. These benefits make encapsulated probiotics an essential component in the formulation of dietary supplements and functional foods.[12] Encapsulation methods involve trapping or adhering drugs to a matrix or surface, or bonding drugs to the material. Molecular weight and stability play crucial roles in determining their effectiveness and safety. Larger molecules may pose challenges, and interactions between drugs and capsules influence encapsulation. Various capsule production methods have been developed, influenced by factors like particle size, reproducibility, and final product stability.[13] Alginate is the most widely used biopolymer for microencapsulation because it is inexpensive, non-toxic, forms gentle matrices with calcium chloride, and easily entraps living microbial cells. It is also a food additive that is widely acknowledged and can be used in food without any harmful effects. Its low stability in the presence of chelating agents and in acidic environments below pH 2 restricts its application.[14] Coating alginate beads with chitosan enhances the stability and vitality of encapsulated probiotic microbes. The colon's microbiota breaks down chitosan and solubilizes alginate gel by retaining calcium ions.[15]

Probiotic foods are also sources of other nutritional compounds, such as antioxidants, fibre, unsaturated fatty acids, minerals, or vitamins and offer synergistic effects to health.[16] *Clitoria ternatea* is a flower rich in antioxidants, flavonoids, and phenolic compounds, with antimicrobial properties. It is used in nanoencapsulation to improve the stability and bioavailability of bioactive compounds, protect sensitive ingredients from oxidation, and enhance controlled nutrient release in food and pharmaceutical applications.[17] Compared to synthetic encapsulating agents, *C. ternatea* offers natural antioxidant protection, higher encapsulation efficiency for anthocyanins, and better bioavailability than conventional microencapsulation techniques.[18] Although *Clitoria ternatea* has been investigated for its antioxidant and antibacterial characteristics, its utilization in chitosan–alginate-based nanoencapsulation for probiotic stabilization and ecotoxicity evaluation is insufficiently reported. In this study, the viability of *L. acidophilus* with probiotic qualities was examined, along with the isolation and encapsulation of *C. ternatea* extract coated chitosan-*L. acidophilus* nanocapsules (CT-CS-LA-NC). The polydispersity index, zeta potential, thermogravimetric analysis (TGA), scanning electron microscopy (SEM), Fourier transform infrared spectroscopy (FTIR), and encapsulation efficiency were used to examine the structural and functional properties followed by the antioxidant properties, gastrointestinal survivability and storage stability of probiotic nanocapsules. The environmental compatibility was evaluated through ecotoxicity profiling and molecular interaction modeling.

2. Materials and methods

2.1 Reagents and chemicals

All reagents and chemicals for nanocapsule preparation and other biological assays including protein profiling study were purchased from Sigma. Hi-Media, India, provided the culture medium used for the microbiological analysis (extra-pure analytical grade). All the chemicals were obtained with high purity and were used without any further purification.

2.2 Isolation of *Lactobacillus acidophilus* from curd

The probiotic strain used in this study was isolated from fresh homemade curd prepared from cow milk obtained from a local milk store in Purasawalkam, Chennai. The sample was collected in a sterile flask, and stored under refrigerated conditions (4 °

C). The initial pH of the curd sample was measured to be 4.7. Initially, 10 g of curd sample was homogenised in 90 mL of sterile distilled water to make a 10^{-1} (w/v) stock suspension. Serial dilutions were performed on this suspension by transferring 1 mL of the preceding dilution into 9 mL of sterile distilled water to generate a range of 10^{-2} to 10^{-5}. Then, 0.1 mL of each serially diluted sample was poured into already pre-solidified MRS agar and incubated at 37 °C for 24 hours with constant homogeneous shaking under aerobic conditions. The bacterial isolates were purified using the streak plate method and kept for four weeks at 4 °C on agar slants until characterisation. Gram stain and acid production tests were used to further analyse the isolate's cellular morphology and staining properties.[19]

2.3 Identification of probiotic strain

The isolated *Lactobacillus* species is identified using morphological (Gram staining, spore test, and motility test), biochemical (indole production test and catalase test), and molecular characterization (16S rRNA sequencing) for the identification of lactic acid bacteria isolates. Plates with white and creamy colonies (presumptive for LAB) were selected and purified through three successive transfers on MRS medium.[20]

2.3.1 16S rRNA sequencing analysis. Further confirmation of bacterial strain was identified by 16S rRNA sequencing. Genomic DNA was prepared using universal primers, and PCR amplification of 16S rRNA was carried out. TCR products were sequenced using universal primers. A PCR reaction mixture (50 μL) comprising 5 μL of dNTPs, 1 μL of each primer rD1 and fD1, 1 μL of the extracted DNA, 5 μL of PCR buffer and 1 μL of Taq DNA polymerase, was used to amplify the 16S rRNA gene.

PCR amplicons and a heat cycler were used for the amplification process. The 16S rRNA gene sequence reported in this study was identified with NCBI sequences. After the sequences were aligned, MEGA version 4.0 was used to create a phylogenetic tree.[21]

2.3.2 Viable inoculum preparation of *L. acidophilus*. For inoculum preparation, the slant culture of *Lactobacillus* was inoculated in the sterilized MRS broth (pH 6.2) at 37 °C for 24 h. The homogenised suspension was then centrifuged for 10 minutes at 10 000 rpm. The biomass that was obtained from *L. acidophilus* was centrifuged and rinsed with 0.1 M phosphate-buffered saline. The cells were then resuspended in phosphate buffered saline. The washed cells served as the inoculum source.[22]

2.4 Preparation of *C. ternatea* extract coated chitosan-*L. acidophilus* nanocapsules (CT-CS-LA-NC)

C. ternatea (butterfly pea flowers) was purchased from local retail outlets. They were subjected to a pretreatment process by double washing in running tap water and distilled water to remove impurities. Ten grams of butterfly pea flower petals were homogenized and soaked in 100 mL of distilled water. The mixture was then placed on a rotary shaker for 72 hours. After this period, the suspension was gently shaken and filtered through filter paper to remove the solids. The filtered crude extract was concentrated using a rotary evaporator set at 50 °C (TOP-300RE) to a constant weight and the resulting dry mass yield was measured as 5.059 mg mL^{-1}; the concentration was determined by dividing the final mass by the initial volume using a gravimetric method.[22] The concentrated extract from the butterfly pea flower petals was collected in screw-cap vials for the formulation of nanocapsules. The qualitative analysis of aqueous *C. ternatea* flower extract was assessed by the standardized method reported by Chakraborty *et al.* (2017).[23]

In a typical procedure, nano-encapsulated chitosan and probiotic (*Lactobacillus*) with plant extract (*C. ternatea*) was formulated. 25 mL of 1.2% sodium alginate and 1 mL of *C. ternatea* extract and 0.5 mL of probiotic suspension (CT-CS-LA-NC) were drawn into a 10 mm diameter Pasteur pipette. These were then carefully dispensed drop by drop into a solution containing 100 mL of 10% $CaCl_2$ and 1 mL of Tween 20, forming beads. Droplets were immersed in a calcium chloride solution for 30 minutes. The beads were retrieved, rinsed twice with sterile water, and blotted in a Petri dish to remove any remaining water, resulting in surface-dried beads.[24]

2.5 Encapsulation efficiency

The encapsulation efficiency (EE) of coating materials refers to their ability to hold or encapsulate core materials within the capsule, and it is a key feature of wall materials. After the CT-CS-LA-NC beads dissolved, the encapsulated probiotic cells were counted directly to determine the encapsulation efficiency (EE). 1 mL of the initial probiotic mixture was plated onto MRS agar after being serially diluted in sterile phosphate-buffered saline (PBS, pH 7.2). After 48 hours of incubation at 37 °C, the initial cell concentration (N_i) was calculated by counting the colony-forming units (CFU) on the plates. For the encapsulated cells, 1 g of CT-CS-LA-NC beads was homogenized using a sterile glass homogenizer and added to 9 mL of sterile PBS, and then 1 mL of the solution was serially diluted in sterile PBS and plated on MRS agar. The colonies were counted after 48 hours of incubation at 37 °C to determine the final cell concentration (N_f).[25] The encapsulation efficiency was calculated using the following formula:

$$\mathrm{EE}\ (\%) = (N_f/N_i) \times 100$$

where N_i is the initial cell concentration before encapsulation and N_f is the final cell concentration after encapsulation.

2.6 Characterization of CT-CS-LA-NC

The structural and functional properties of the nanocapsule were determined by using appropriate analytical techniques. The findings provided essential insights into the capsule's stability and release mechanisms, facilitating prospective uses in preservation. The data indicate that the nanocapsule may improve efficacy while minimizing side effects.

2.6.1 Particle size and polydispersity index (PDI). The dynamic light scattering (DLS) method was used to measure the particle size and polydispersity index (PDI) using a Malvern Zetasizer Nano ZS90 (Malvern Instruments Ltd, Worcestershire,

UK). To obtain the ideal scattering intensity, all samples were diluted 1 : 100 with distilled water before analysis. Measurements were conducted in triplicate at a regulated temperature of 25 ± 2 °C, with the detector oriented at a 90° scattering angle. The *Z*-average diameter (mean particle size) and PDI were determined by averaging the measurements done in triplicate.[26]

2.6.2 Zeta potential (ZP) analysis. The zeta potential of solid lipid nanoparticles was measured using the Malvern Zetasizer Nano ZS90 (Malvern Instruments Ltd, Worcestershire, UK) at a temperature of 25 ± 2 °C. This apparatus measures the zeta potential using the electrophoretic mobility of the particles by combination of two measurement methods like electrophoresis and laser Doppler analysis. It shows that the physical stability of the SLNs is predicted. Prior to measurement, each sample was diluted in distilled water, pH was maintained at 7.0 and the results were calculated by average measurements in triplicate.[26]

2.6.3 Fourier transform infrared spectroscopy. Functional groups were recorded by FTIR using a Thermo Fisher Scientific Nicolet-iS50 spectrophotometer equipped with a micro attenuated total reflectance (ATR) accessory and a diamond disc as an internal reflection element.

2.6.4 Scanning electron microscopy (SEM). The surface morphology of the freeze-dried nanocapsules was analysed using a scanning electron microscope (SEM). This analysis was performed with the assistance of a focused electron beam in a high-vacuum environment using a SUPRA 55 CARL ZEISS (Germany) microscope, which offers a resolution of 200 Å and a magnification range of 35 to 10 000×.

2.6.5 TGA (thermogravimetric analysis). The surface temperature meter (SDT) Q600 V20.9 Build 20 was used for thermogravimetric analysis (TGA) and differential scanning calorimetry (DSC) of the nanocapsule in the temperature range of 37 °C to 700 °C using a heating rate of 7 °C min^{-1} in nitrogen.

2.7 Antioxidant activity

2.7.1 DPPH free radical scavenging activity. The DPPH radical scavenging assay, as outlined by Blois (1958),[27] and the modified method by Rahman *et al.* (2015)[28] were used to evaluate the CT-CS-LA-NC methanolic extract's and the standard's capacity to scavenge free radicals. A 0.1 mM DPPH in methanol solution was made, and 100 μL of this solution was added with the CT-CS-LA-NC methanolic extract at several concentrations (20–100 μg mL^{-1}). In methanol solution, DPPH appears violet/purple but fades to yellow when antioxidants are present. At 517 nm, the absorbance was measured. Using the following formula, the percentage of DPPH radical scavenging activity was determined:

$$\%\ \text{DPPH free radical scavenging activity} = [(A_0 - A_1)/(A_0)]$$

where A_0 is the absorbance of the control and A_1 is the absorbance of the extractives/standard. Then the % of inhibition was plotted against concentration, and from the graph, IC_{50} was calculated using linear regression. The experiment was repeated three times at each concentration.

2.8 Antibacterial activity

Antibacterial activity of the nanocapsule was tested against *Bacillus subtilis* (ATCC 6051) and *Escherichia coli* (ATCC 25922) adopting a well diffusion assay. All the experiments were carried out with free *L. acidophilus*, nano-encapsulated *L. acidophilus*, and secretors of free *L. acidophilus* and nano-encapsulated *L. acidophilus* separately. Inocula of respective treatments were prepared in MRS broth incubated at 37 °C for 18 hours. The secretory product of *L. acidophilus* was obtained from the culture supernatant of the respective treatment group (inoculated MRS broth centrifuged at 8000 rpm for 10 min); the collected supernatant was syringe filtered and used as the source for antibacterial activity. Inocula of the respective bacterial cultures prepared in MRS broth were uniformly spread on the sterile MRS agar media. Wells were made on the swabbed agar using a sterile gel puncture (8 mm). 100 μL of viable inocula of *L. acidophilus* thus prepared was added to the wells. For 24 hours, the seeded plates were incubated at 37 °C.[29] The plates were examined for zones of inhibition following the incubation period.

2.9 Evaluation of acid tolerance

The modified acid tolerance test was performed as described previously by Ehrmann *et al.* (2002).[30] Acid stress condition was created by adjusting the pH of the MRS broth to 2.5 using 1 N HCl in addition. The inoculum thus prepared was added to 100 mL of sterile MRS broth in various conical flasks at concentrations (v/v) ranging from 0.5 mL to 2.5 mL, respectively, and incubated at 37 °C under shaking conditions. Additionally, the CT-CS-LA-NC was suspended in the MRS broth at concentrations (w/v) varying from 0.5 g to 2.5 g and incubated for 48 hours. These treatment groups were observed and compared against a control group. The turbidity of the culture media was monitored at several time intervals (12 hours, 24 hours, and 36 hours). After the incubation period, the optical densities (OD 570 nm) were recorded at 12-hour intervals for 48 hours. The negative control, which was only the media, showed no growth. The same procedure was repeated for all the treatment and control groups under the same experimental conditions, respectively. All tests were carried out in triplicate.

2.10 Evaluation of bile tolerance

A previously adapted technique by Akmal *et al.* (2022)[31] was used to assess bile tolerance. The simulated bile conditions were prepared by adding 0.3 g in 100 mL (0.3% w/v) of MRS broth and using a 1 M sodium hydroxide solution to adjust the pH to 7.5. After preparation, 100 mL of sterile MRS broth in various conical flasks were filled with the inoculum at concentrations ranging from 0.5% (v/v) to 2.5% (v/v), respectively, and shaken while being incubated at 37 °C. After being dissolved in the MRS broth at concentrations varying from 0.5% (w/v) to 2.5% (w/v), the CT-CS-LA-NC was incubated for 36 hours. These treatment groups were observed and contrasted with the control group. There was no growth in the negative control, which consisted solely of the media. Then, a spectrophotometer was used to

measure the track bacterial growth at 560 nm. Every experiment was run in triplicate.

2.11 Storage stability

The stability and storage conditions of the free probiotic and CT-CS-LC-NC were comparatively evaluated over 28 days, *via* a method adapted from Thinkohkaew *et al.* (2024).[32] Both the encapsulated alginate beads and the free probiotic cell suspension were stored in sterile conical tubes containing 0.5% sterile sodium chloride (NaCl) solution at 4 °C. The viability of the probiotics in the free suspension and the beads was assessed at different time periods, including 7, 14, 21, and 28 days. The encapsulated samples were dissolved in NaCl to release cells. After serial dilutions and the dot-plating method, the viable cell count was measured on the MRS agar plates. The plates were incubated at 37 °C for 48 hours before colony-forming units (CFU) were counted. The survival rate for each sample at each time point was then determined and compared to the initial viable cell count to determine the probiotic viability under refrigerated conditions.

2.12 Ecotoxicity assessment of CT-CS-LA-NC

The ecotoxic effect of the fabricated nanocapsule was determined by measuring the phytotoxic effect and soil parameters.

2.12.1 Seed germination exposure. The *Vigna mungo* seeds were first rinsed thoroughly in deionized water and further surface sterilized with a 70% ethanol solution to reduce microbial contamination. For treatment, seeds were immersed for 24 hours in a homogenized blend of CT-CS-LA-NC. This essential soaking procedure was carried out in darkness at ambient temperature to emulate standard pre-sowing treatment conditions while regulating light conditions. 16 *Vigna mungo* seeds were carefully dried after treatment, and the germination assay was started by transferring them to Petri dishes with a filter paper. After that, they were kept at room temperature in a dark environment. Distilled water was sprayed twice a day in a fine mist with a 12-hour gap between applications to maintain ideal moisture levels adapted from the method followed by Abbas *et al.* (2024).[33] All of the tests were done in triplicate.

2.12.2 SDS-PAGE (sodium dodecyl sulfate-polyacrylamide gel electrophoresis). According to Fling and Gregerson (1986),[34] SDS-PAGE was used to assess the differences in the protein profile of plant tissue taken from the respective treatment and control groups. For extraction of proteins, black gram seeds were ground to fine powder. Sample buffer (1.5 M Tris–HCl, 1% SDS, 30% glycerol and 2% β-mercapto ethanol, pH 6.8) was mixed with protein extracts in a 1 : 1 ratio. Protein movement in the gel was observed by adding Bromophenol Blue (BPB) as a tracking dye to the sample buffer. The control and treated samples' crude protein extracts were dissolved in sodium phosphate buffer (pH 7.5) and centrifuged for three minutes at 10 000 rpm. Soluble proteins were separated using stacking and linear gradient acrylamide separating gels at a constant current until the tracking dye reached the separating gel's edge. Coomassie Brilliant Blue R-250 (CBBR) staining was applied to the gels. 0.05 M Tris–glycine buffer was used for the electrophoresis, which was carried out at 10 °C (pH 8.3) until the sample bands crossed the stacking layer. The protein bands were visualized.

2.13 *In silico* docking

The 3D structures of the proteins were obtained from the RCSB PDB database (https://www.rcsb.org/pdb) using the following PDB IDs: 7K41, 8AE1. The ligand molecules anthocyanin (PubChem CID: 154824275), chitosan (PubChem CID: 441477), and lactic acid (PubChem CID: 612) were obtained from the PubChem website (https://pubchem.ncbi.nlm.nih.gov). The target proteins' optimal protein–ligand interaction sites were found using CB-Dock software, which also computes the target proteins' size and shape using a curvature-based cavity identification technique and performs docking using AutoDock Vina software. Based on Vina scores, CB-Dock evaluates the binding modes and provides an interactive three-dimensional model of them.[35]

2.14 Statistical analysis

All data were obtained from experiments carried out at least in duplicate. The results were compared using one-way analysis of variance (ANOVA) followed by Duncan's *post hoc* (Prism software version 5.0). Results were considered significant when $P < 0.05$.

3. Results and discussion

3.1 Isolation and identification of *L. acidophilus*

The probiotic strain *L. acidophilus* used in this study was isolated from the curd by a culture-dependent method. The serially diluted curd sample was spread plated on sterile MRS agar followed by incubation under optimum conditions (identification of the isolate was done by morphological and biochemical properties shown in Table 1). The *L. acidophilus* was isolated from curd. The selected bacterial strain was identified by morphological and biochemical characterization as *L. acidophilus*. Morphologically, the single colonies were circular and creamy white. The bacteria were Gram-positive rods and cocci-shaped, and were further observed under a phase contrast microscope as shown in Fig. S1. This study revealed Gram-positive, non-spore-forming rods showing a negative result (red colour): all the isolated strains were found to be catalase-negative (no bubble formation) and indole test-negative bacteria. This is in agreement with the study conducted by

Table 1 Morphological and biochemical characteristics of *L. acidophilus*

Characterization	Result
Gram staining	Gram positive
Spore test	Non-spore forming rods
Motility test	Non-motile
Indole production test	Negative
Catalase test	Negative

Table 2 Qualitative analysis of the plant extracts of *Clitoria ternatea* to screen for the presence of phytochemicals

S. no.	Phytochemical analysis	Presence/absence
1	Alkaloids	+
2	Flavonoids	+
3	Steroids	−
4	Phenol	+
5	Tannin	+
6	Saponin	−

Rozos *et al.* (2018).[36] Thus, the results obtained coincided with *L. acidophilus* strain characteristics.

3.1.1 16S rRNA sequencing and phylogenetic analysis. After the confirmation, the isolated *L. acidophilus* was stored on MRS agar slant for further studies. The *L. acidophilus* used for the nanocapsules was inoculated and prepared in sterile MRS broth. *L. acidophilus* was seeded, and the broth was centrifuged, followed by collecting the cell pellets. Cells were washed with sterile PBS, and the washed cells were used as the source of inoculum. The final yield of the inoculate was found to be 1.0% w/v; the healthy inoculum thus prepared was used for further studies.

The 16S rRNA gene sequence of isolated strains showed 96% similarity to *L. acidophilus*. All isolated strains corresponding to *Lactobacillus* were considered to be the best match based on top hit similarity.[37] The sequence has been deposited in the NCBI GenBank database under accession number PX470079. The phylogenetic trees were designed in the bootstrap neighbor-joining (NJ) method (Fig. S2) based on 16S rRNA gene sequencing.

3.2 Preparation of *C. ternatea* extract coated chitosan-*L. acidophilus* nanocapsules (CT-CS-LA-NC)

C. ternatea extract-coated chitosan-*L. acidophilus* nanocapsules were prepared by the simple *in situ* principle of *C. ternatea*, which was readily extracted in distilled water under ambient conditions, and the final yield of the metabolite was found to be 1.029 g L^{-1}. The extracted metabolite was stored in screw cap vials and used for further studies. Phytochemical screening of *C. ternatea* leaves indicated the presence of active components such as alkaloids, flavonoids, tannins, phenols, and saponins, with steroids being absent, as shown in Table 2. In a related study, Neda *et al.* (2013)[38] detailed the phytochemical compounds and nutritional composition found in *C. ternatea* flowers.

A simple *in situ* dispersion method was employed for the preparation of nanocapsules. Opaque probiotic nanocapsules with a sphere-like structure (Fig. 1) and highly stable characteristics were fabricated using *C. ternatea* extract, chitosan polymer, and *L. acidophilus*. Synthesized CT-CS-LA-NC was characterised by techniques like scanning electron microscopy, Fourier transform infrared spectroscopy, and thermogravimetric analysis. Among the various substances, chitosan is an important polymer used for the encapsulation of probiotic-stabilised nanocapsules, revealing enhanced biological activities. Chitosan improves solubility, stability and resistance to degradation, which offers controlled drug delivery to specific sites and has enhanced antimicrobial properties.[39,40]

Fig. 1 *C. ternatea* extract coated chitosan-*L. acidophilus* nanocapsule (CT-CS-LA-NC).

3.3 Encapsulation efficiency of CT-CS-LA-NC

The encapsulation efficiency (EE) of the CT-CS-LA-NC beads was found to be 98.43% (Fig. S3). The CT-CS-LA-NC coating material's significant efficacy in preserving the probiotic cells during the encapsulation process is due to its high efficiency. The results of the present study agreed with Afzaal *et al.* (2020)[41] who reported that sodium alginate microbead encapsulating probiotics are 98% more effectively than carrageenan. The alginate matrix entraps more cells than the other material, but both materials entrap the necessary number of cells. Probiotic survival is increased by encapsulation with alginate and whey protein, suggesting that efficient probiotic consumption is necessary for colonization in the colon.

3.4 Characterization techniques

3.4.1 Polydispersity index. Dynamic light scattering (DLS) analysis confirmed the formation of the CT-CS-LA-NC composite within the targeted nanometer size range. The *Z*-average size measured was 162 nm, categorizing the overall distribution within the sub-micron scale, which is optimal for targeted delivery. The distribution exhibited a notable and significant peak, validating the synthesis of chitosan nanocapsules with a mean diameter of 91.1 nm (Fig. S4). The results indicate effective encapsulation of *L. acidophilus* within a stable, nano-structured delivery system.

3.4.2 Zeta potential. According to the surface zeta potential of CT-CS-LA-NC, which was measured to be -54.7 ± 0.32 mV, it can be concluded that the nanoparticles in the dispersant (water) exhibit a high degree of electrostatic stability (Fig. S5). This analysis is essential for interpreting the colloidal behaviour of chitosan NPs. The significant negative charge indicates that the particles repel each other, consequently minimizing aggregation. Stability in chitosan formulations may be due to coating or loading anionic components, such as phenolics from *C. ternatea* extract or other stabilizing excipients, resulting in a stable nanocapsule rather than a cationic core. The research conducted by Weng *et al.* (2022)[42] indicated that the surface zeta

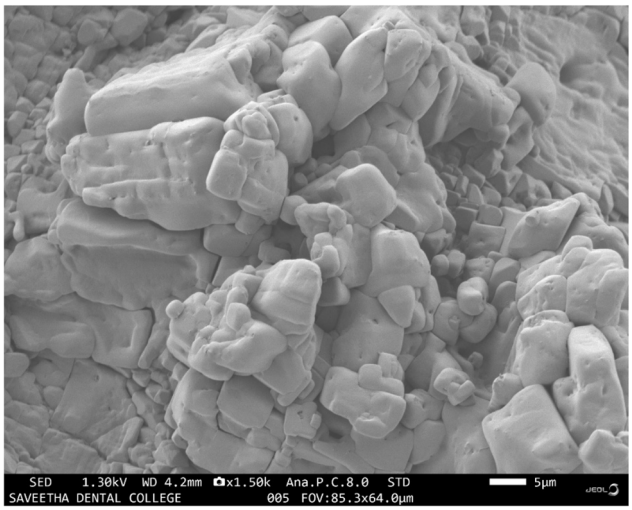

Fig. 2 SEM micrograph of CT-CS-LA-NC.

potential of *L. acidophilus* cell envelope LA/TCS@PLGA-NPs was −21.3 ± 0.46 mV. The observed increase in zeta potential indicates a charge screening effect attributed to the coated envelope. A study conducted by Barrera-Necha *et al.* (2018)[43] demonstrated that chitosan nanoparticles, when combined with botanical extracts, exhibited a zeta potential value of −43.8 mV.

3.4.3 Scanning electron microscopy (SEM). SEM reveals significant details about the surface morphology of the nano-encapsulated composite of plant extract (*Clitoria ternatea*), probiotic (*Lactobacillus*), and chitosan. The surface topology of the CT-CS-LA-NC nanocapsules, as shown in Fig. 2, was analysed using SEM. With its densely packed, complex surface topology, the SEM micrograph displays irregular particles with consistent shape homogeneity, indicating good nanocomposite encapsulation and stability. The relatively smooth surface morphology suggests a uniform distribution of the *Clitoria ternatea* extract and probiotics within the chitosan matrix, indicating an efficient encapsulation process and strong integration (Fig. 2). According to the SEM image, the average size of the synthesized nanocapsule is 5 μm and the image suggests that the structures found are either uniform or non-uniform and fall within the nanometre range.[44] Based on this SEM analysis, the nanoencapsulation process appears to have successfully formed composite structures, suggesting efficient interaction between the chitosan, probiotic, and plant extract which could influence the release dynamics in pharmacological applications.[45]

3.4.4 Fourier transform infrared spectroscopy (FTIR). The vibrational characteristics of the chitosan–alginate nanocapsule (CS–NC) control shows a broad and intense peak at 3344.49 cm^{-1}, reflecting the merged stretching vibrations of hydroxyl (O–H) and amine (N–H) groups inherent to the chitosan framework. The peaks in the fingerprint region further confirm the polymer's structure. The strong band at 1587.15 cm^{-1} is linked to N–H bending, and the characteristic absorption bands at 1424.25 cm^{-1} and 1330.35 cm^{-1} are linked to C–H bending and C–N stretching, respectively. The band at 1052.50 cm^{-1} indicates C–O–C glycosidic linkage and C–O stretching, confirming chitosan's polysaccharide composition and structure.

The FTIR spectroscopy results of the synthesized chitosan-probiotic-*Clitoria ternatea*-nanocapsule (CT-CS-LA-NC) revealed absorption peaks across the range of 720 cm^{-1} to 3350 cm^{-1}, signifying molecular interactions and the presence of various functional groups (Fig. 3). The peak at 3350 cm^{-1} might be related to O–H stretching, which indicates that hydroxyl groups are present. Chitosan mostly consists of N–H and O–H stretching, amide bands, C–O–C stretching, and C–H stretching, among several other peaks.[46,47] Broad absorption peaks at 2922 cm^{-1} and 2855 cm^{-1} suggest C=O carboxyl stretching and typical C–H stretching in alkanes, respectively. A sharp peak at 1582 cm^{-1} could correspond to C=C stretching vibrations in aromatic compounds.[48] The distinct peaks at 1421 cm^{-1} and 1326 cm^{-1} are often indicative of C–C stretching (Kumar and Mohideen, 2024).[47] Additionally, the absorption at

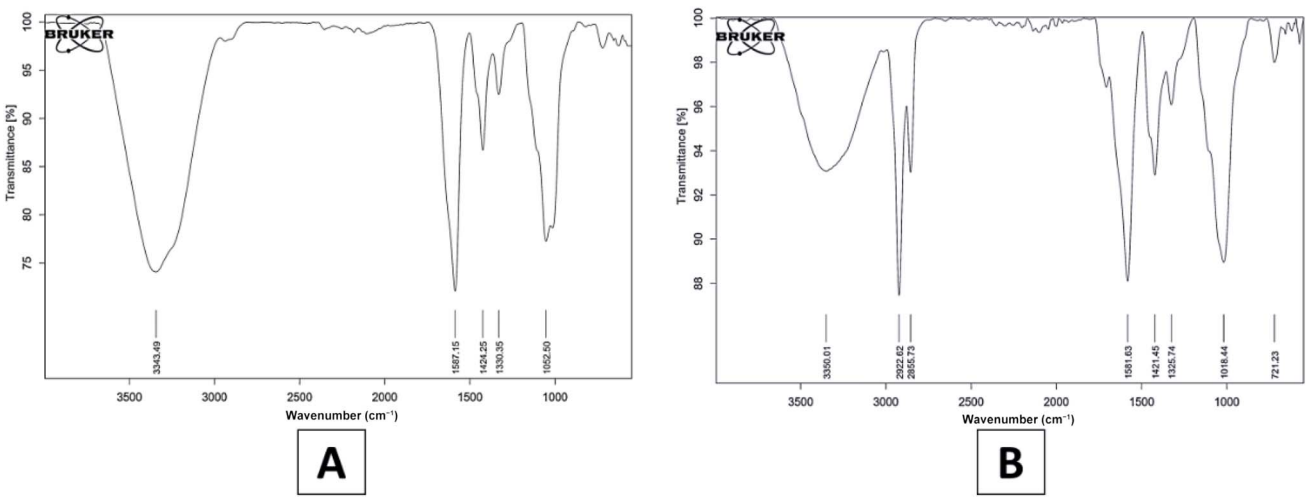

Fig. 3 FTIR spectrum of (A) CS–NC and (B) CT-CS-LA-NC.

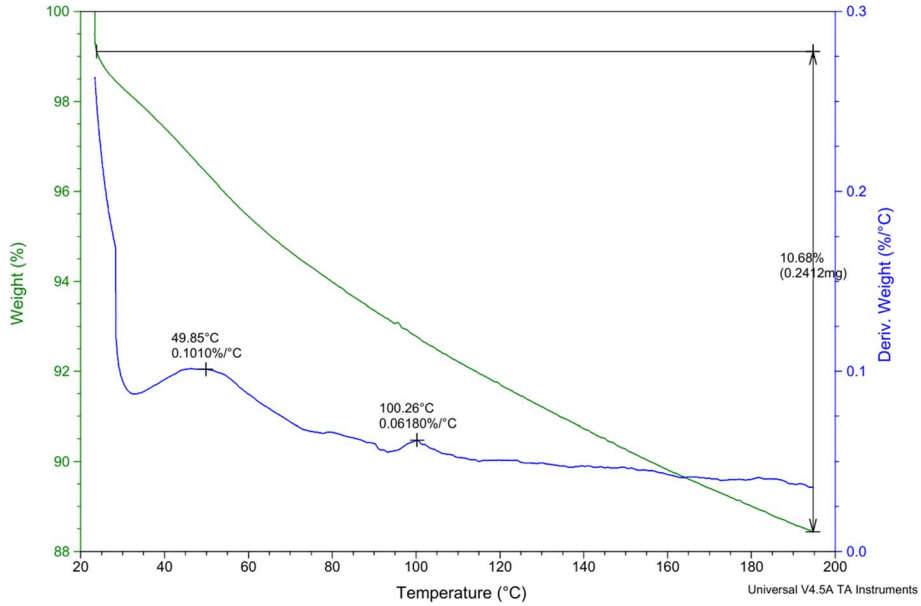

Fig. 4 TGA analysis of CT-CS-LA-NC.

1018.44 cm^{-1} might represent C–N stretching vibrations found in ethers or alcohols, signifying the presence of aliphatic amines.[49] Lastly, the peak at 721 cm^{-1} is commonly associated with C–H rocking modes, further confirming the molecular characteristics of the nano-encapsulated structure. Senthil Kumar *et al.* (2024)[50] reported that this is due to glycosidic linkages in chitosan, polysaccharides, and the bacterial cell wall of *Lactobacillus fermentum*. Chitosan (CS) is the reference peak, and shifts in existing peaks can be attributed to interactions between compounds. This can be explained by the glycosidic bonds present in polysaccharides, present in chitosan as well as the bacterial cell wall of *Lactobacillus fermentum*.[50] With chitosan (CS) as a reference peak, we can confirm the presence of chitosan in the synthesised NPs and mild shifts in existing peaks could be linked to interactions between the bacterial components.[51] The FTIR spectra of the CS–NC (Fig. 3A) control and the CT-CS-LA-NC (Fig. 3B) show significant structural modifications. The CT-CS-LA-NC spectrum reveals two bands at 2922 cm^{-1} and 2855 cm^{-1}, indicating the presence of organic compounds such as lipids, proteins from *L. acidophilus*, and organic acids from *C. ternatea*. These peaks are absent in the pure chitosan control. The shift in the N–H bending/amide II peak from 1587.15 cm^{-1} in the control to 1581.63 cm^{-1} in the formed sample confirms the encapsulation of the plant extract. The most significant change is the shift of the characteristic chitosan C–O/C–N stretching peak from 1052.50 cm^{-1} to 1018.44 cm^{-1}. This shift suggests that the encapsulated components and chitosan have strong molecular interactions, which confirms the successful chemical integration and stabilization of the nanocomposite.

3.4.5 Thermogravimetric analysis. The thermal stability of the synthesised nanocapsule (CT-CS-LA-NC) was determined by thermogravimetric analysis, which measures weight loss in relation to rising temperature.[52] The weight of the nanocapsule gradually decreases as the temperature rises when the sample is heated from 20 °C to 200 °C at intervals of 10 °C (Fig. 4).

The sample weighed 2.2590 mg initially, and as the temperature increased, the mass changed. At 49.85 °C, a slight weight loss of 0.1010% was noted during the initial decomposition stage. This implies the elimination of any remaining moisture or volatile components, which is common for materials based on chitosan, according to Zhang *et al.*'s (2021) study.[53] This significant loss suggests the breakdown of polymeric structures, such as chitosan and probiotic encapsulation materials, due to thermal degradation. The weight percentage dropped to 0.0618% in the second decomposition stage at 100.26 °C indicating further water loss or slight degradation of low-molecular-weight compounds. At end of the experiment, a final retained weight of 10.68% was recorded, indicating a total weight loss of 0.2412 mg. The results obtained by Hong *et al.* (2007)[54] confirm the existence of several thermal degradation phases and indicate that nanoencapsulation improves thermal stability by postponing degradation relative to pure chitosan.

3.5 Antibacterial activity

Antibacterial activity was tested against *E. coli* and *B. subtilis* using a well-diffusion assay. The assay was performed with viable inocula of the respective *L. acidophilus* treatment groups, including their secretory products. The results showed that all treatments inhibited the growth of both bacterial strains. The nano-encapsulated *L. acidophilus* and its secretory product exhibited the largest zones of inhibition for *Escherichia coli*, measuring 14.2 ± 0.26 cm and 14.3 ± 0.27 mm, respectively. The zone of inhibition formed by the secretory product of the free *L. acidophilus* was 13.1 ± 0.17 cm, whereas the smallest zone was established by the free *L. acidophilus* itself, measuring 12 ± 0.19 mm for *Bacillus subtilis* as shown in Table 3. The nano-

Table 3 Antibacterial activity of free *L. acidophilus* and nano-encapsulated *L. acidophilus* against *Escherichia coli* and *Bacillus subtillis*[a]

S. no.	Treatment	Zone of inhibition (mm)	
		Escherichia coli (ATCC 25922)	*Bacillus subtillis* (ATCC 6051)
1	Free *L. acidophilus*	12 ± 0.19[c]	13 ± 0.19[c]
2	Nano-encapsulated *L. acidophilus*	14.2 ± 0.26[a]	15.1 ± 0.24[a]
3	Secretory product of free *L. acidophilus*	13.1 ± 0.17[b]	13.4 ± 0.21[c]
4	Secretory product of nanoencapsulated *L. acidophilus*	14.3 ± 0.27[a]	14.4 ± 0.32[b]

[a] Values are presented as the mean ± standard error of the mean ($n = 3$). Different letters in the same columns denote statistical significance ($P < 0.05$) according to Duncan's multiple range test, which was performed following a significant one-way ANOVA.

encapsulated *L. acidophilus* and its secretory product were similarly quite effective, which exhibited a zone of inhibition of 15.1 ± 0.24 mm and 14.4 ± 0.32 mm. The inhibition of the free *L. acidophilus* and its secretory product was similar, with zones of 13 ± 0.19 mm and 13.4 ± 0.21 mm, respectively. Similar to the viable inocula, the secretory products from both free and encapsulated formulations showed growth inhibition. These findings are consistent with those of Soltani *et al.* (2022)[55] who reported that the most significant growth inhibition zones were associated with the extracts of *L. acidophilus* (16 mm) and *L. casei* (15 mm) strains. The secretome of both *Lactobacillus* strains exhibited a greater growth inhibition zone.

3.6 Antioxidant activity

3.6.1 DPPH free radical scavenging activity. DPPH is a stable free radical that changes color to purple when dissolved in methanol. The reaction between free radicals and antioxidants changes their colour from purple to yellow, which in turn changes their properties. The concentration of the assessed free *L. acidophilus*, CT-CS-LA-NC, and ascorbic acid varied between 200 and 1000 μg mL^{-1}. The antioxidant activity test with DPPH was compared to standard concentrations (ascorbic acid) using a linear regression analysis to assess efficiency and consistency. The DPPH activity graph shows a concentration-dependent rise in free radical scavenging for all three tested materials, with the nanocomposite CT-CS-LA-NC exhibiting the highest antioxidant efficacy across all concentration ranges. At the maximum concentration of 1000 μg mL^{-1}, the CT-CS-LA-NC sample reaches 48.2 ± 1.32% inhibition, showing an increase over the free *L. acidophilus* cells (16.75 ± 0.98%) (Fig. 5). This significant enhancement in activity suggests a synergistic effect resulting from the incorporation of *Clitoria ternatea* (CT) into the CT-CS-LA (NC), indicating that the prepared nanocomposite exhibits a high antioxidant delivery system compared to the standard and the free probiotic cells. The IC_{50} of CT-CS-LA-NC was determined to be 28.04 μg mL^{-1}, whereas the IC_{50} of free *L. acidophilus* was 3.22 μg mL^{-1}, and both were compared to the standard ascorbic acid concentration ($IC_{50} = 1.61$ μg mL^{-1}). The antioxidant activity of *C. ternatea* flower solvent or water extracts has been measured previously by Jeyaraj *et al.* (2022),[18] and the anthocyanin-rich proportion has more efficacy than the crude extracts, with IC_{50} values of 1.24 μg mL^{-1}, respectively. *C. ternatea* and chitosan both have natural antioxidant and antibacterial properties. Flavonoids present in *C. ternatea* also have a wide range of antimicrobial effects. Together, these three components exhibit strong synergistic resistance.[56]

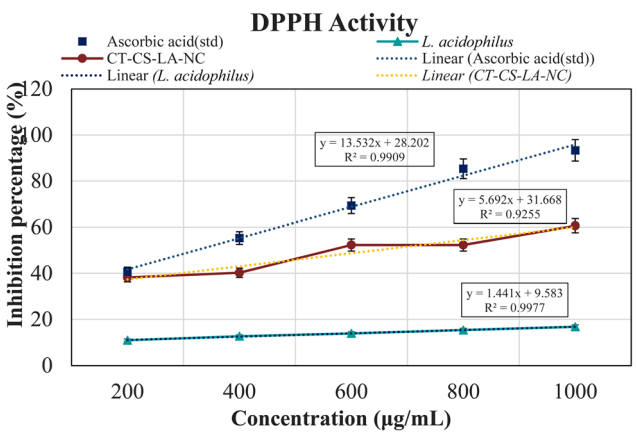

Fig. 5 DPPH assay of CT-CS-LA-NC. (Values are presented as the mean ± standard error of the mean ($n = 3$). Significance at <0.05.)

3.7 Viability of free *L. acidophilus* and CT-CS-LA-NC under acidic conditions

Probiotic bacteria are typically delivered in food systems and must be acid tolerant to survive in the human gastrointestinal tract. The average time from entry to release from the stomach is ninety minutes, though this can vary depending on other digestive processes (Ding and Shah, 2009).[14] Encapsulation improves the survival of probiotic bacteria by providing a protective barrier against harsh environmental conditions, such as the stomach's low pH. This barrier protects the cell membrane and cell wall from being destroyed right away, allowing the bacteria to travel through the gastric environment and into the intestine.[57]

In this acid tolerance study, the survival of free *Lactobacillus acidophilus* and nano-encapsulated CT-CS-LA-NC was assessed under simulated gastric conditions at pH 2.5 and pH 3.5 over 12, 24, and 36 hours is shown in Tables S1 and S2. The concentration of free *L. acidophilus* and CT-CS-LA-NC was varied from 0.5 mL to 2.5 mL. Initially, at a pH of 2.5, the acid resistance of free *L. acidophilus* was moderate over 12 hours, with survival rates varying from 12.08 ± 0.10 to 37.80 ± 0.21. The nano-encapsulated CT-CS-LA-NC showed a similar survival rate, ranging from 1.07 ± 0.12 to 36.49 ± 0.34. Free cells showed

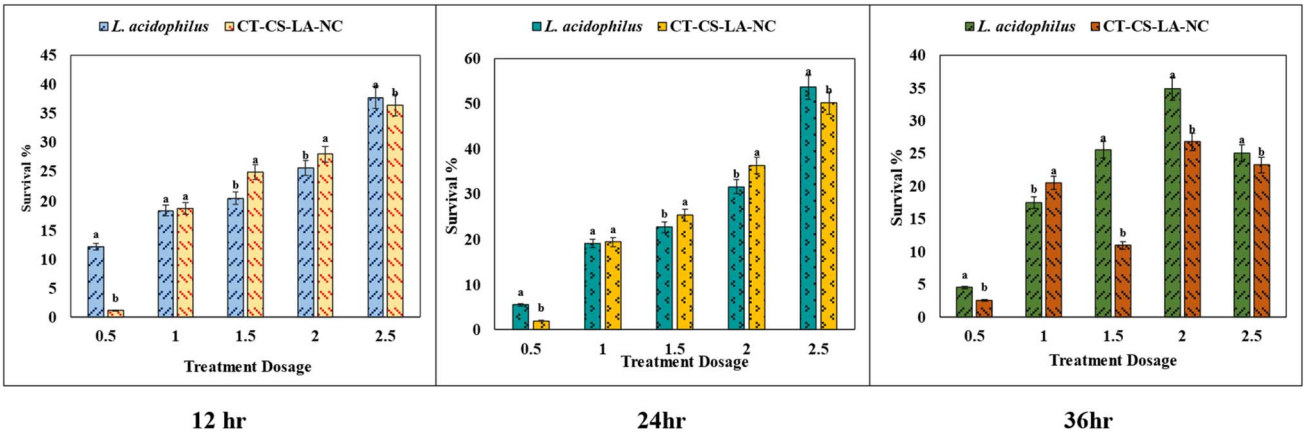

Fig. 6 Viability of free *L. acidophilus* and CT-CS-LA-NC at pH 2.5 at different time intervals (12, 24, and 36 h). The *X*-axis represents the treatment dosage added to 100 mL of MRS broth. For *L. acidophilus*, dosages are 0.5–2.5 mL. For CT-CS-LA-NC, dosages are 0.5–2.5 g. (Values are presented as the mean ± standard error of the mean ($n = 3$). Different letters denote statistical significance ($P < 0.05$) according to Duncan's multiple range test, which was performed following a significant one-way ANOVA.)

better viability of 4.51 ± 0.21 to 25.12 ± 0.16 than the nano-encapsulated cells (2.58 ± 0.15 to 23.26 ± 0.16) after 24 hours of acid exposure. The lower total viable count compared to the free cells may result from the probiotic's gradual and prolonged release from the encapsulation. However, the most significant difference was seen after 36 hours (Fig. 6). Encapsulated cells showed a highly significant survivability rate of 60.93 ± 0.68 at 2.5 mL. In contrast, the survival of free *L. acidophilus* peaked at only 45 ± 0.13.

At pH 3.5, CT-CS-LA-NC maintained similar vitality ranging from 1.93 ± 0.18 to 50.23 ± 0.43 after 12 hours of exposure whereas free *L. acidophilus* also showed similar vitality (5.47 ± 0.24 to 36.68 ± 0.26). Free cell survivability decreased at 24 hours (4.85 ± 0.02 to 9.80 ± 0.08). After 36 hours, CT-CS-LA-NC showed 76.46 ± 0.60 (2 mL), exceeding free cells (65.42 ± 0.73) and exhibiting enhanced acid tolerance. The survivability of CT-CS-LA-NC was greatly improved confirming the enhanced acid tolerance (60.93 ± 0.68) at 2.5 mL after 36 hours, compared to 45 ± 0.13 for free *L. acidophilus*, indicating the high efficiency of the encapsulated *L. acidophilus* (Fig. 7).

These results correspond with prior research. Varela-Pérez *et al.* (2022)[58] indicated that nanoencapsulation improves probiotic survival under acidic conditions. Arratia-Quijada *et al.* (2024)[59] examined persistent acid tolerance in encapsulated strains. Argyri *et al.* (2012)[60] highlighted that resistance to low pH is specific to strains, employing pH 2.5 to identify acid-tolerant *Lactobacilli*. The results indicate the survival rate at different concentrations and time intervals, showing CT-CS-LA-NC's efficiency in preserving probiotic viability under simulated gastrointestinal conditions. Chitosan acts as a prebiotic, providing nourishment for probiotics such as *L. acidophilus* in the large intestine.[61] The synbiotic effect – the combination of a probiotic and a prebiotic—substantially enhances the colonization and therapeutic advantages of the encapsulated bacteria. The synergistic relationship between the components of the product enhances probiotic viability, stability, and

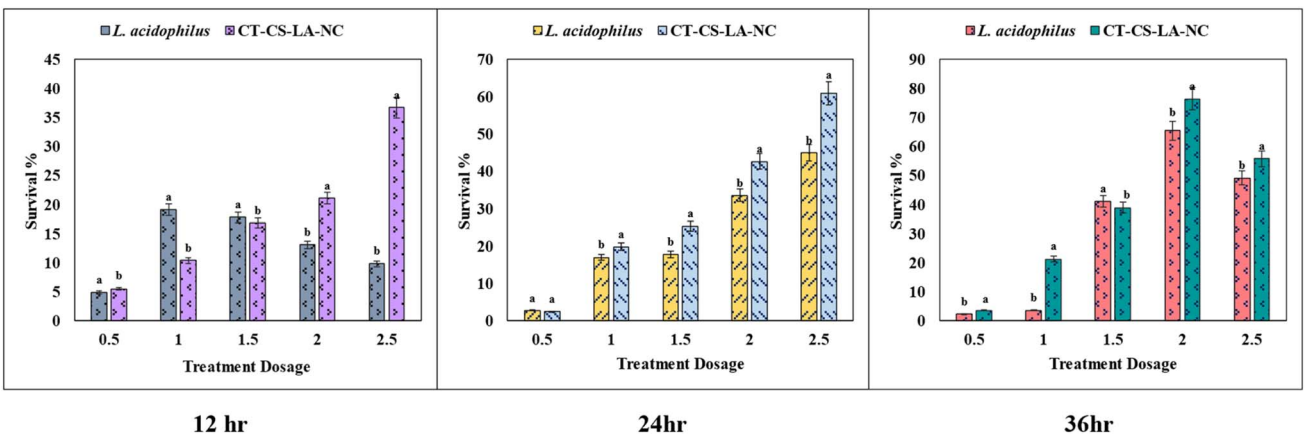

Fig. 7 Viability of free *L. acidophilus* and CT-CS-LA-NC at pH 3.5 at different time intervals (12, 24, and 36 h). The *X*-axis represents the treatment dosage added to 100 mL of MRS broth. For *L. acidophilus*, dosages are 0.5–2.5 mL. For CT-CS-LA-NC, dosages are 0.5–2.5 g. (Values are presented as the mean ± standard error of the mean ($n = 3$). Different letters denote statistical significance ($P < 0.05$) according to Duncan's multiple range test, which was performed following a significant one-way ANOVA.)

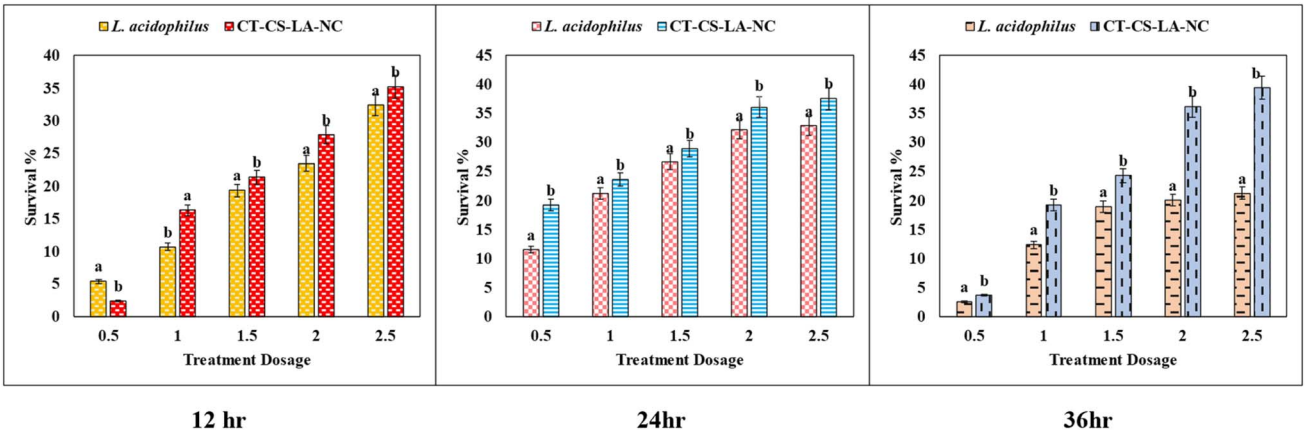

Fig. 8 Viability of free *L. acidophilus* and CT-CS-LA-NC at pH 7.5 at different time intervals (12, 24, and 36 h). The *X*-axis represents the treatment dosage added to 100 mL of MRS broth. For *L. acidophilus*, dosages are 0.5–2.5 mL. For CT-CS-LA-NC, dosages are 0.5–2.5 g. (Values are presented as the mean ± standard error of the mean ($n = 3$). Different letters denote statistical significance ($P < 0.05$) according to Duncan's multiple range test, which was performed following a significant one-way ANOVA.)

therapeutic potential, providing a robust protective effect against gut pathogens, ensuring successful delivery of *L. acidophilus*.[62]

3.8 Viability of free *L. acidophilus* and CT-CS-LA-NC under bile conditions

The survival rates of both free and nano-encapsulated *L. acidophilus* (CT-CS-LA-NC) at two pH values (2.5 and 3.5) over 12, 24, and 36 hours were investigated in this bile tolerance study as shown in Table S3. At a low concentration of 0.5 mL, the tolerance of the free *L. acidophilus* cells was significantly higher than that of the nano-encapsulated cells (5.39 ± 0.13). This implies that the encapsulation might slowly dissolve or activate. However, the nano-encapsulated CT-CS-LA-NC cells showed a noticeably higher tolerance when the concentrations were raised to a higher level (between 1 and 2.5 mL). The CT-CS-LA-NC maximum tolerance at 2.5 mL was 35.24 ± 0.3, greater than the free cell maximum tolerance of 32.41 ± 0.12.

After 24 hours of exposure, the slow-release profile of CT-CS-LA-NC was noticeably superior to that of free *L. acidophilus*. Across a range of nanoencapsulation concentrations (0.5 mL to 2.5 mL), CT-CS-LA-NC demonstrated significantly higher survival rates. CT-CS-LA-NC exhibited a survival rate of 19.25 ± 0.15 at the lowest concentration of 0.5 mL, whereas free cells only showed an 11.56 ± 0.21 survival rate (Fig. 8). As exposure duration increases, nano-encapsulation significantly enhances protection against bile tolerance, as shown by its consistent performance across all of the various concentrations that were assessed. After 36 hours, the highest survivability rates were found in encapsulated cells. At all concentrations, CT-CS-LA-NC's tolerance was significantly greater than that of free *L. acidophilus*. The survival of free *L. acidophilus* was only 21.29 ± 0.13, while the encapsulated cells demonstrated a survivability of 39.46 ± 0.68 at 2.5 mL. This extremely significant difference highlights the high effectiveness of the encapsulated *L. acidophilus* (CT-CS-LA-NC) in resisting the harsh environment of bile acids, particularly at higher concentrations and for longer periods of time.

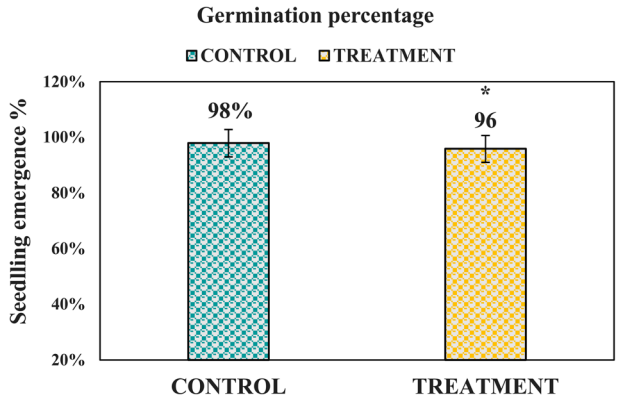

Fig. 9 Seedling germination of *Vigna mungo*. Significance at (*$P < 0.05$).

3.9 Ecotoxicity assessment of CT-CS-LA-NC

3.9.1 Seed germination assay. *Vigna mungo* treated with 5% CT-CS-LA-NC showed a promotion in plant growth. Results indicate that CT-CS-LA-NC has not shown any toxic effect on seedling emergence. CT-CS-LA-NC-treated seeds showed 96% of the seedling's emergence in *Vigna mungo* (Fig. 9). The control group showed a 100% growth rate. These findings suggest that using CT-CS-LA-NC enhances seedling emergence. The difference of only 2.19% between the treatment and control groups suggests that the nanocapsules had no significant inhibitory effect on seed viability. The control set showed 98 ± 0.21% gemination. The GP value of 96.81% ($P \leq 0.05$) in the treatment set indicates that nearly all of the treated seeds germinated, supporting the conclusion that the CT-CS-LA NC treatment did not inhibit or interfere with the biological processes involved in seedling germination.

3.9.2 Protein profiling study using SDS-PAGE. SDS-PAGE analysis of protein extracted from *Vigna mungo* provided insights into the impact of CT-CS-LA-NC treatment on protein

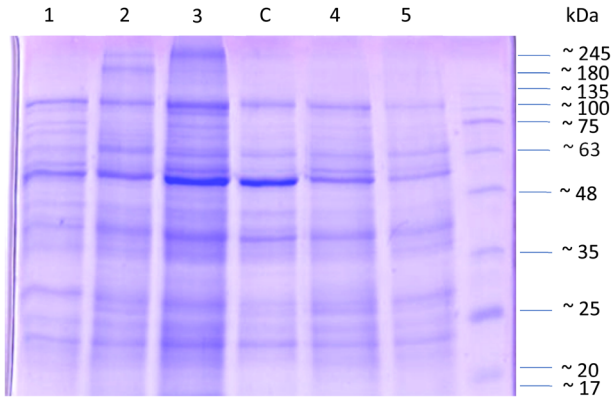

Fig. 10 SDS-PAGE analysis of protein extracted from *Vigna mungo*.

expression (Fig. 10). Molecular weight estimation using reference markers (245 kDa to 17 kDa) revealed 15 distinct protein bands, with fainter bands between 35 kDa and 25 kDa suggesting potential regulatory protein modifications. According to the study by Torio *et al.* (2011)[63] the major storage protein, 8Sα globulin, identified as a trimer of subunits at 49 kDa, was prominently expressed in lanes 2, 3, and 5, as well as in the control. Comparisons between control and treated groups demonstrated shifts in protein profiles, highlighting the effects of CT-CS-LA-NC interaction.[64] SDS-PAGE effectively facilitated molecular weight characterization and regulatory insights into protein expression in *Vigna mungo*.

3.10 Storage stability

The probiotic cells encased in an encapsulating matrix must endure severe conditions, including external factors and the gastrointestinal tract, while also preserving their viability during storage. The storage temperature has a major impact on the viability of the cells during the storage time. This study involved the storage of free *L. acidophilus* cells and encapsulated cells at a refrigerated temperature of 4 °C. Fig. 11 depicts the storage stability of free *L. acidophilus* and CT-CS-LA-NC probiotics when stored at a refrigeration temperature of 4 °C for a duration of 28 days. The viability of the free cells showed rapid

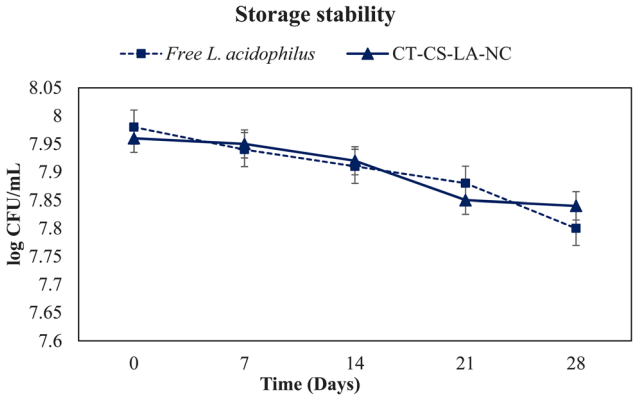

Fig. 11 Storage stability of free *L. acidophilus* and CT-CS-LA-NC at 4 °C for 28 days. The presented values are expressed as means ± SD ($n = 3$).

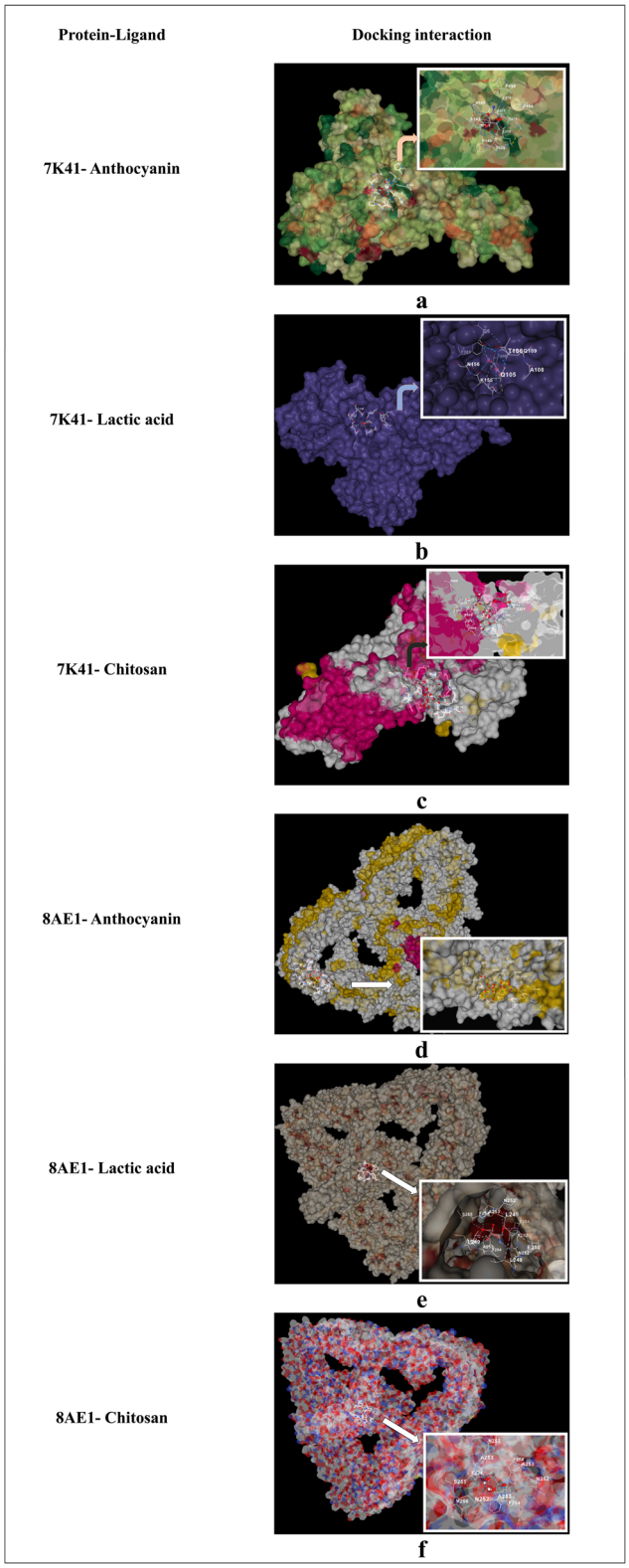

Fig. 12 (a–f) *In silico* docking interaction of proteins (7K41, 8AE1) with ligands (anthocyanin, lactic acid, and chitosan).

decline, with the survival rate decreasing from an initial 7.98 to 7.8 $\log_{10}$ CFU per mL by the end of 28 days. However, the CT-CS-LA-NC encapsulated cells also had similar higher survival rates,

Table 4 *In silico* docking analysis of proteins and ligands using CB-Dock

Protein	Ligand	Interaction score (kcal mol^{-1})	Cavity volume
7K41	Anthocyanin	−9.4	2633
7K41	Lactic acid	−4.1	2633
7K41	Chitosan	−5.2	534
8AE1	Anthocyanin	−9.6	893
8AE1	Lactic acid	−3.8	2141
8AE1	Chitosan	−5.4	2163

retaining 7.84 $\log_{10}$ CFU per mL viability after 7 days and maintaining more than half of their initial population up to 14 days after the 28 days. Probiotic viability and storage durability are enhanced by the steady and gradual release of cells from the coating material, chitosan biopolymer, which traps *L. acidophilus* inside the alginate. Fareez *et al.* (2014)[65] reported that while decreasing viability loss at 75 and 90 °C, Alg–XG–Ch increased the storage durability of *L. plantarum* LAB12 at 4 °C, and *L. plantarum* LAB12, combined in Alg–XG–Ch, might be used as a new functional food ingredient with health benefits.

3.11 *In silico* docking

In the present study, the docking analysis focused on identifying the molecular interactions between two proteins associated with probiotics, O-GlcNAcase (7K41) and S-layer associated protein (SlpA) (8AE1), along with three significant compounds from the nanoencapsulated system, such as anthocyanin, lactic acid, and chitosan (Fig. 12). Anthocyanin has a high binding affinity for O-GlcNAcase (7K41) and SlpA (8AE1), with interaction scores of −9.4 kcal mol^{-1} and −9.6 kcal mol^{-1}, respectively. These interaction scores show that anthocyanin forms stable complexes with proteins, indicating its potential to impact their functions, which is consistent with previous studies on its bioactivity, which is associated with its ability to interact with proteins. According to the study by Hidalgo *et al.* (2012)[66] anthocyanin contributes to the preservation of gastrointestinal health by modulating the microbial composition of the gut and providing antioxidant activity in the large intestine. Chitosan exhibited significant interaction scores of −5.2 kcal mol^{-1} for O-GlcNAcase and −5.4 kcal mol^{-1} for SlpA, shown in Table 4, which indicates the distinct binding sites (534 for 7K41 and 2163 for 8AE1) on each protein. Its interaction with SlpA, a key component of the bacterial cell wall, supports its role in protecting the cell membrane. Likewise, lactic acid also had notable interaction scores of −4.1 kcal mol^{-1} (7K41) and −3.8 kcal mol^{-1} (8AE1). These *in silico* findings explain the nano-encapsulated system's synergistic effects and emphasize the molecular interactions between anthocyanin, chitosan, and lactic acid.

4. Conclusion

The study successfully demonstrates the nanoencapsulation of *Lactobacillus acidophilus* using chitosan and *Clitoria ternatea* extract (CT-CS-LA-NC). The effective encapsulation of *Lactobacillus acidophilus* using this approach presents new possibilities for its use as a biopreservative in functional foods, drinks, and nutraceuticals. This method's effective encapsulation of *Lactobacillus acidophilus* creates potential opportunities for its use as a biopreservative in nutraceuticals, functional foods, and drinks. Nanocapsules with improved thermal and acid stability would facilitate the development of novel probiotic-enriched products, such as juices, food products, and dietary supplements, which are traditionally difficult to formulate with probiotics. It may also be able to prolong the shelf life of perishable goods, eliminating the need for artificial preservatives, given its proven antibacterial qualities against common food pathogens like *B. subtilis* and *E. coli*. CT-CS-LA-NC provides a versatile and sustainable solution that offers both functional health advantages and enhanced product stability in response to the growing consumer demand for natural products.

Consent for publication

We consent to publish in this journal.

Author contributions

M. Lavanya: data curation, formal analysis, investigation, methodology, software, original manuscript writing. S. Karthick Raja Namasivayam: conceptualization, supervision, investigation, manuscript review and editing.

Conflicts of interest

We declare no conflict of interest.

Data availability

The data will be made available on request from the authors.

Supplementary information (SI): comprehensive characterization and stability data for *Lactobacillus acidophilus* and the CT-CS-LA-NC formulation. It includes Gram staining, phylogenetic tree analysis, and physicochemical characterization *via* encapsulation efficiency, particle size distribution (DLS), and zeta potential measurements. Additionally, the file contains detailed comparative viability data for free *L. acidophilus* and CT-CS-LA-NC across varying pH levels (2.5, 3.5, and 7.5) and treatment dosages over 12, 24, and 36-hour intervals. See DOI: https://doi.org/10.1039/d5fb00833f.

References

1 S. K. Amit, Md. M. Uddin, R. Rahman, S. M. R. Islam and M. S. Khan, *Agric. Food Secur.*, 2017, **6**, 51.
2 M. Martínez-Ballesta, Á. Gil-Izquierdo, C. García-Viguera and R. Domínguez-Perles, *Foods*, 2018, **7**, 72.
3 T. Didari, S. Solki, S. Mozaffari, S. Nikfar and M. Abdollahi, *Expert Opin. Drug Saf.*, 2014, **13**, 227–239.

4 R. R. Watson and V. R. Preedy, *Probiotics, Prebiotics, and Synbiotics: Bioactive Foods in Health Promotion*, Academic Press, 2015.
5 S. Fijan, *Int. J. Environ. Res. Public Health*, 2014, **11**, 4745–4767.
6 P. A. Mackowiak, *Front. Public Health*, 2013, **1**, 52.
7 A. Latif, A. Shehzad, S. Niazi, A. Zahid, W. Ashraf, M. W. Iqbal, A. Rehman, T. Riaz, R. M. Aadil, I. M. Khan, F. Özogul, J. M. Rocha, T. Esatbeyoglu and S. A. Korma, *Front. Microbiol.*, 2023, **14**, 1216674.
8 K. Prajapati, K. Bisani, H. Prajapati, S. Prajapati, D. Agrawal, S. Singh, M. Saraf and D. Goswami, *Syst. Microbiol. Biomanuf.*, 2023, **4**, 386–406.
9 M. Bernatek, H. Sommermeyer, A. Wojtyła, J. Piątek and S. Lachowicz-Wiśniewska, *J. Health Inequal.*, 2023, **9**, 194–200.
10 M. L. Marco and S. Tachon, *Curr. Opin. Biotechnol.*, 2012, **24**, 207–213.
11 A. Pugazhendhi, M. A. Alshehri, S. Kandasamy, P. K. Sarangi and A. Sharma, *Food Chem.*, 2024, **464**, 141762.
12 L. Stasiak-Różańska, A. Berthold-Pluta, A. S. Pluta, K. Dasiewicz and M. Garbowska, *Int. J. Environ. Res. Public Health*, 2021, **18**, 1108.
13 K. V. M. Rameez, P. Santhoshkumar, K. S. Yoha and J. A. Moses, *Curr. Res. Nutr. Food Sci. J*, 2024, **12**, 539–560.
14 W. K. Ding and N. P. Shah, *J. Food Sci.*, 2009, **74**, 100–107.
15 M. Chávarri, I. Marañón, R. Ares, F. C. Ibáñez, F. Marzo and M. Del Carmen Villarán, *Int. J. Food Microbiol.*, 2010, **142**, 185–189.
16 D. Dahiya and P. S. Nigam, *Fermentation*, 2022, **8**, 303.
17 M. Pateiro, B. Gómez, P. E. S. Munekata, F. J. Barba, P. Putnik, D. B. Kovačević and J. M. Lorenzo, *Molecules*, 2021, **26**, 1547.
18 E. J. Jeyaraj, Y. Y. Lim and W. S. Choo, *Sci. Rep.*, 2022, **12**, 14890.
19 A. Menconi, G. Kallapura, J. D. Latorre, M. J. Morgan, N. R. Pumford, B. M. Hargis and G. Tellez, *Biosci. Microbiota, Food Health*, 2014, **33**, 25–30.
20 C. A. Okafor and P. E. Ekwueme, *Asian Food Sci. J.*, 2024, **23**, 95–104.
21 B. Tilahun, A. Tesfaye, D. Muleta, A. Bahiru, Z. Terefework and G. Wessel, *Int. J. Food Sci.*, 2018, **2018**, 1–7.
22 G. C. V. Gamage, Y. Y. Lim and W. S. Choo, *Front. Plant Sci.*, 2021, **12**, 792303.
23 S. Chakraborty, S. Sahoo, A. Bhagat and S. Dixit, *Zenodo (CERN Eur. Organ. Nucl. Res.)*, 2017, **5**, 197–208.
24 H. Choukaife, A. A. Doolaanea and M. Alfatama, *Pharmaceuticals*, 2020, **13**, 335.
25 D. Arepally, R. S. Reddy and T. K. Goswami, *Food Funct.*, 2020, **11**, 8694–8706.
26 M. Cassayre, D. T. De Souza, M. Claeys-Bruno, A. Altié, P. Piccerelle and C. Sauzet, *Nanomaterials*, 2025, **15**, 1034.
27 M. S. Blois, *Nature*, 1958, **181**, 1199–1200.
28 Md. M. Rahman, Md. B. Islam, M. Biswas and A. H. M. K. Alam, *BMC Res. Notes*, 2015, **8**, 621.
29 N. Soltani, S. Abbasi, S. Baghaeifar, E. Taheri, M. F. S. Jadid, P. Emami, K. Abolhasani and F. Aslanshirzadeh, *Biotechnol. Rep.*, 2022, **36**, e00760.
30 M. A. Ehrmann, P. Kurzak, J. Bauer and R. F. Vogel, *J. Appl. Microbiol.*, 2002, **92**, 966–975.
31 U. Akmal, I. Ghori, A. M. Elasbali, B. Alharbi, A. Farid, A. S. Alamri, M. Muzammal, S. M. B. Asdaq, M. A. E. Naiel and S. Ghazanfar, *Fermentation*, 2022, **8**, 328.
32 K. Thinkohkaew, N. Aumphaiphensiri, T. Tangamornsiri, N. Niamsiri, P. Potiyaraj and I. Suppavorasatit, *J. Agric. Food Res.*, 2024, **18**, 101405.
33 Z. Abbas, M. A. Hassan, W. Huang, H. Yu, M. Xu, X. Chang, X. Fang and L. Liu, Influence of magnesium oxide (MgO) nanoparticles on maize (Zea mays L.), *Agronomy*, 2024, **14**(3), 617, DOI: 10.3390/agronomy14030617.
34 S. P. Fling and D. S. Gregerson, *Anal. Biochem.*, 1986, **155**, 83–88.
35 Y. Liu, M. Grimm, W.-T. Dai, M.-C. Hou, Z.-X. Xiao and Y. Cao, *Acta Pharmacol. Sin.*, 2019, **41**, 138–144.
36 G. Rozos, C. Voidarou, E. Stavropoulou, I. Skoufos, A. Tzora, A. Alexopoulos and E. Bezirtzoglou, *Front. Microbiol.*, 2018, **9**, 517.
37 G. Sumalata and M. Shiva Prakash, *J. Adv. Sci. Res.*, 2023, **14**, 40–49.
38 G. D. Neda, M. S. Rabeta and M. T. Ong, *Int. Food Res. J.*, 2013, **20**, 1229–1234.
39 P. R. Deshmukh, A. Joshi, C. Vikhar, S. S. Khdabadi and M. Tawar, *Syst. Rev. Pharm.*, 2022, **13**, 685–693.
40 Y. Pérez-Pacheco, B. Tylkowski and R. García-Valls, *Molecules*, 2025, **30**, 252.
41 M. Afzaal, F. Saeed, M. Saeed, M. Azam, S. Hussain, A. A. Mohamed, M. S. Alamri and F. M. Anjum, *Int. J. Food Prop.*, 2020, **23**, 1899–1912.
42 L. Weng, L. Wu, R. Guo, J. Ye, W. Liang, W. Wu, L. Chen and D. Yang, *J. Nanobiotechnol.*, 2022, **20**(1), 356, DOI: 10.1186/s12951-022-01563-x.
43 L. L. Barrera-Necha, Z. N. Correa-Pacheco, S. Bautista-Baños, M. Hernández-López, J. E. M. Jiménez and A. F. M. Mejía, *Adv. Microbiol.*, 2018, **08**(04), 286–296, DOI: 10.4236/aim.2018.84019.
44 M. A. Ahghari, M. R. Ahghari, M. Kamalzare and A. Maleki, *Sci. Rep.*, 2022, **12**, 10491.
45 S. Vijayaram, R. Sinha, C. Faggio, E. Ringø and C.-C. Chou, *AIMS Microbiol.*, 2024, **10**, 986–1023.
46 J. J. Joseph, D. Sangeetha and T. Gomathi, *Int. J. Biol. Macromol.*, 2015, **82**, 952–958.
47 S. S. Kumar and S. S. Mohideen, *Sci. Rep.*, 2024, **14**, 21182.
48 M. C. Curk, F. Peledan and J. C. Hubert, *FEMS Microbiol. Lett.*, 1994, **123**, 241–248.
49 R. V. Mathai, J. C. Mitra and S. K. Sar, *Rasayan J. Chem.*, 2021, **14**, 1423–1434.
50 S. Senthil Kumar and S. S. Mohideen, *Sci. Rep.*, 2024, **14**, 21182.
51 R. Shanmugam, T. Munusamy, S. Jayakodi, K. A. Al-Ghanim, M. Nicoletti, N. Sachivkina and M. Govindarajan, *Fermentation*, 2023, **9**, 413.

52 S. K. R. Namasivayam, M. Manohar, J. A. Kumar, K. Samrat, A. Kande, R. S. A. Bharani, C. Jayaprakash and S. Lokesh, *Environ. Res.*, 2022, **212**, 113386.
53 Y. Zhang, Y. Wu, M. Yang, G. Zhang and H. Ju, *Materials*, 2021, **14**, 5538.
54 P. Hong, S. Li, C. Ou, C. Li, L. Yang and C. Zhang, *J. Appl. Polym. Sci.*, 2007, **105**, 547–551.
55 N. Soltani, S. Abbasi, S. Baghaeifar, E. Taheri, M. F. S. Jadid, P. Emami, K. Abolhasani and F. Aslanshirzadeh, *Biotechnol. Rep.*, 2022, **36**, e00760.
56 G. I. Edo, A. N. Mafe, N. F. Razooqi, E. C. Umelo, T. S. Gaaz, E. F. Isoje, U. A. Igbuku, P. O. Akpoghelie, R. A. Opiti, A. E. A. Essaghah, D. S. Ahmed, H. Umar and D. U. Ozsahin, *Des. Monomers Polym.*, 2024, **28**, 1–34.
57 N. Sulistiani, I. Novarina, N. Inawati, A. Dinoto, H. Julistiono, R. Handayani and S. Saputra, *IOP Conf. Ser.: Earth Environ. Sci.*, 2020, **572**, 012026.
58 A. Varela-Pérez, O. O. Romero-Chapol, A. G. Castillo-Olmos, H. S. García, M. L. Suárez-Quiroz, J. Singh, C. Y. Figueroa-Hernández, R. Viveros-Contreras and C. Cano-Sarmiento, *Foods*, 2022, **11**, 740.
59 J. Arratia-Quijada, K. Nuño, V. Ruíz-Santoyo and B. A. Andrade-Espinoza, *J. Funct. Foods*, 2024, **116**, 106192.
60 A. A. Argyri, G. Zoumpopoulou, K.-A. G. Karatzas, E. Tsakalidou, G.-J. E. Nychas, E. Z. Panagou and C. C. Tassou, *Food Microbiol.*, 2012, **33**, 282–291.
61 S. S. Kumar and S. S. Mohideen, *Sci. Rep.*, 2024, **14**, 21182.
62 S. Nigam, D. V. Ram and A. A. M. Kumar, *Int. J. Pharm. Sci. Rev. Res.*, 2022, 154–160.
63 M. A. O. Torio, M. Adachi, R. N. Garcia, K. Prak, N. Maruyama, S. Utsumi and E. M. Tecson-Mendoza, *Food Res. Int.*, 2011, **44**, 2984–2990.
64 Ma. C. Gamis, L. Y. Uy, A. Laurena, W. Hurtada and M. A. Torio, *Appl. Sci.*, 2020, **10**, 8787.
65 I. M. Fareez, S. M. Lim, R. K. Mishra and K. Ramasamy, *Int. J. Biol. Macromol.*, 2014, **72**, 1419–1428.
66 M. Hidalgo, M. J. Oruna-Concha, S. Kolida, G. E. Walton, S. Kallithraka, J. P. E. Spencer, G. R. Gibson and S. De Pascual-Teresa, *J. Agric. Food Chem.*, 2012, **60**, 3882–3890.